ISSN 1392–1320 MATERIALS SCIENCE (MEDŽIAGOTYRA). Vol. 25, No. 3. 2019

The Influences of SiO_2 on the Sintering Behavior and the Properties of Na^+-β/β''-Al_2O_3 Solid Electrolyte

Sung-Tae LEE, Dae-Han LEE, Sung-Ki LIM *

Department of Materials Ehemistry and Engineering, Konkuk University, 120, Neungdong-ro, Gwangjin-gu, 143-701, Seoul, Republic of Korea

crossref http://dx.doi.org/10.5755/j01.ms.25.3.14246

Received 24 February 2016; accepted 15 May 2016

SiO_2-doped Na^+-β/β″-Al_2O_3 was synthesized via a solid-state reaction, and the relationship between the SiO_2 content and properties of Na^+-β/β″-Al_2O_3 was investigated. Respective specimens were doped with 0 – 5 wt.% SiO_2 as a liquid phase sintering promotor and sintered. The specimens were characterized by XRD, SEM, densimeter and impedance analyzer. In the sintered samples, the phase fraction of β″-Al_2O_3 decreased as the SiO_2 content increased, whereas the relative sintered density was enhanced with the inclusion of less than 0.7 wt.% SiO_2. The relative sintered density of Na^+- β/β″-Al_2O_3 sintered specimen with 0.7 wt.% SiO_2 doping reached 99.2 % of the theoretical density and the sintered density decreased when the amount of SiO_2 was larger than 1 wt.% result from excessive liquid-phase formation during sintering. Similarly, the ionic conductivity of SiO_2-doped Na^+-β/β″-Al_2O_3 was enhanced by doping with a small amount of SiO_2, whereas the addition of more than 1 wt.% SiO_2 negatively affected the ionic conductivity of Na^+-β/β″-Al_2O_3 due to a decrease in the sintered density and unfavorable phase relationship.

Keywords: Na^+-β/β″-Al_2O_3, solid electrolyte, SiO_2, liquid phase sintering, ionic conductivity.

1. INTRODUCTION

Na^+-β/β″-Al_2O_3 has been widely utilized as a solid electrolyte in sodium/sulfur batteries for electric vehicles and for storage of excess electricity [1, 2], where the Na^+ ions act as charge carriers. Na^+-β/β″-Al_2O_3 is characterized by a highly ionic nature and low electronic conductivity, and extensive research has been dedicated to exploiting these features for practical purposes.

Generally, Na^+-β/β″-Al_2O_3 is prepared by a conventional solid-state reaction, in which the raw materials are initially prepared by mechanical mixing [3 – 6] followed by calcination. The thus-synthesized β/β″-Al_2O_3 powders are converted to green bodies by cold isostatic pressing, slip casting, and uniaxial pressing, and are then sintered [7 – 9].

Synthesis of Na^+-β/β″-Al_2O_3 by the conventional solid-state reaction inevitably requires a long holding time at a high sintering temperature, which leads to the loss of sodium, thereby deleteriously eroding the ionic conductivity of the β/β″-Al_2O_3 ceramics. Small additions of various oxides, such as MgO, TiO_2, MnO_2, and SiO_2 to α-Al_2O_3 have been shown to influence the densification processes by reducing the sintering temperature, suppressing or promoting grain growth, and allowing sintering to theoretical density [10, 11]. Therefore, a variety of oxides, either singly or in combination, is commonly used in the ceramic industry for various purposes, such as for enhancing sintering or for microstructural and mechanical modification. Among these oxides, SiO_2 is well recognized to improve the densification of ceramics by liquid phase sintering. Liquid phase sintering offers an alternative method of overcoming the lack of densification. Numerous studies have shown that the presence of small amounts of SiO_2 strongly influences the microstructure and the properties of α-Al_2O_3 [12 – 18]. However, it has not been conclusively demonstrated that SiO_2 is incorporated as a liquid phase sintering promoter in Na^+-β/β″-Al_2O_3 electrolytes during the powder synthesis step. This study presents the fabrication of SiO_2-doped Na^+-β/β″-Al_2O_3 specimens and evaluates the relationship between the SiO_2 content and the properties of the doped Na^+-β/β″-Al_2O_3.

2. EXPERIMENTAL DETAILS

Na^+-β/β″-Al_2O_3 solid electrolytes doped with SiO_2 were synthesized via a solid-state reaction using commercial powders of α-Al_2O_3 (99.99 %, High Purity Chemicals, Japan), Na_2CO_3 (99 + %, Sigma-Aldrich, USA), $4MgCO_3 \cdot Mg(OH)_2 \cdot 5H_2O$ (99 + %, Sigma-Aldrich, USA), and SiO_2 (99.9 + %, High Purity Chemicals, Japan) as the starting materials. The synthesized Na^+-β/β″-Al_2O_3 powders contained 1.6 wt.% MgO (stabilizer), Na_2O at a $[Na_2O]/[Al_2O_3]$ molar ratio of 1 : 5, and various amounts of SiO_2 ranging from 0 to 5 wt.%.

The starting materials were mixed by ball-milling for 5 h in methanol as the liquid medium; the mixture was then calcined at 1200 °C for 2 h after drying at 90 °C. The calcined powders were molded by application of a uniaxial pressure of 100 bars to obtain the green samples with dimensions of Φ 14 mm × 2 mm. To minimize Na_2O loss, the green samples were buried in MgO crucibles packed with packing powder of already synthesized Na^+-β/β″-Al_2O_3 and sintered at 1600 °C for 30 min.

The phase composition of the calcined and sintered samples was analyzed using an X-ray diffractometer

* Corresponding author. Tel.: +82-2-450-3500; fax: +82-2-444-3490.
E-mail address: *sklim@konkuk.ac.kr* (S.K. Lim)

(XRD, D/max 2200, Rigaku, Japan). XRD analysis was performed at 40 kV and 30 mA using Cu Kα radiation. The relative amounts of the phases were determined by calculating the line intensities of the well-separated peaks of each phase using the following equations [19, 20]:

$$\% \text{ of } \alpha = f(\alpha)/\{f(\alpha)+f(\beta)+f(\beta'')\}\times 100; \quad (1)$$

$$\% \text{ of } \beta = f(\beta)/\{f(\alpha)+f(\beta)+f(\beta'')\}\times 100; \quad (2)$$

$$\% \text{ of } \beta'' = f(\beta'')/\{f(\alpha)+f(\beta)+f(\beta'')\}\times 100; \quad (3)$$

$$f(\alpha) = 1/2\{I_{\alpha(104)}\times 10/9+I_{\alpha(113)}\}; \quad (4)$$

$$f(\beta) = 1/3\{I_{\beta(102)}\times 10/3+I_{\beta(206)}\times 10/3.5+I_{\beta(107)}\times 10/5.5\}; \quad (5)$$

$$f(\beta'') = 1/2\{I_{\beta(10\underline{11})}\times 10/4+I_{\beta''(20\underline{10})}\times 10/8\}, \quad (6)$$

where $I_{\alpha(104),\ \alpha(113)}$ denotes the X-ray intensity of the (104), (113) planes of the α- Al_2O_3 phase, $I_{\beta(102),\ \beta(206),\ \beta(107)}$ represents the X-ray intensity of the (102), (206), (107) planes of the β- Al_2O_3 phase, and $I_{\beta''(10\underline{11}),\ \beta''(20\underline{10})}$ indicates the X-ray intensity of the (10$\underline{11}$), (20$\underline{10}$) planes of the β"-Al_2O_3 phase.

The microstructure of the sintered specimen and the density were assessed by scanning electron microscopy (SEM, Model JSM-6380, Japan) and by using Archimedes method (ASTM 373-88). The ionic conductivities of the sintered specimens were measured by employing blocking silver electrodes using an electrochemical complex impedance analyzer (Zahner, IM6) within the frequency range of 1 Hz to 3 MHz and temperature range of 25 to 350 °C. Sodium conductivities were calculated using Eq. 7.

$$\sigma = L/(R_s \times A) \quad (7)$$

where σ, L, R_s and A denote the ionic conductivity, specimen thickness, impedance of the specimen, and electrode area, respectively.

3. RESULTS AND DISCUSSION

Fig. 1 presents schematic structures of Na^+-β-Al_2O_3 and Na^+-β″-Al_2O_3. The crystalline structure of β″-Al_2O_3 is a rhombohedral structure with an R3m space group with lattice constants of 'a' = 5.614 and 'c' = 33.85 Å. Generally, the 'a' axis is similar to that of the β-Al_2O_3 structure, but the length of its 'c' axis is 1.5 times longer, and the concentration of the alkaline ions on the conduction plane is higher [21, 22]. Fig. 2 shows the projection of β-Al_2O_3 and β″-Al_2O_3 unit cells stacking sequence. The unit cell of β″-Al_2O_3 is 50 % larger than that of β-Al_2O_3 by virtue of the difference in stacking sequence. Adjacent close packed oxide slabs are again held apart by Al-O-Al spacer units, but alternate sodium atom sites lie above and below the plane through the centre of the oxide spacer atoms and the Na^+ ion diffusion path actually encompasses a finite volume (the conduction slab) rather than a plane as in the β-Al_2O_3 structure. β″-Al_2O_3 has a higher sodium content in the conduction slab than β-Al_2O_3, and therefore is more conductive than β-Al_2O_3.

Fig. 3 shows the XRD patterns of the powders doped with different amounts of SiO_2 that were calcined at 1200 °C for 2 h. The Na^+-β phase has the theoretical fomula $Na_2O{\cdot}11Al_2O_3$, or $NaAl_{11}O_{17}$ [23], and the β"-phase has the formula $Na_2O{\cdot}5Al_2O_3$, or $NaAl_5O_8$ [24]. According to Na_2O-Al_2O_3 phase diagram proposed by Fally et al. [25], the β + β"-phases coexist in a region corresponding to the formula $Na_2O{\cdot}nAl_2O_3(5.33 \le n \le 8.5)$. The XRD patterns of all calcined powders conform to the crystalline phase of $NaAl_5O_8$ (JCPDS 31-1262) and $NaAl_{11}O_{17}$ (JCPDS 31-1263). No significant peaks corresponding to SiO_2 were detected in the XRD patterns, which may be due to the low SiO_2 concentration (less than 1 wt.%).

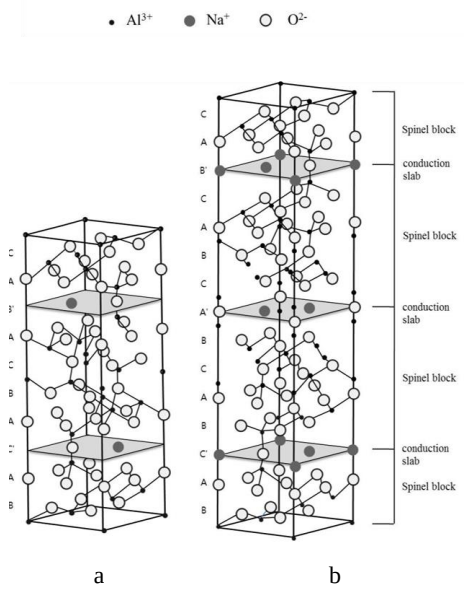

Fig. 1. Perspective drawings of the idealized structures of a – β-Al_2O_3; b – β″-Al_2O_3

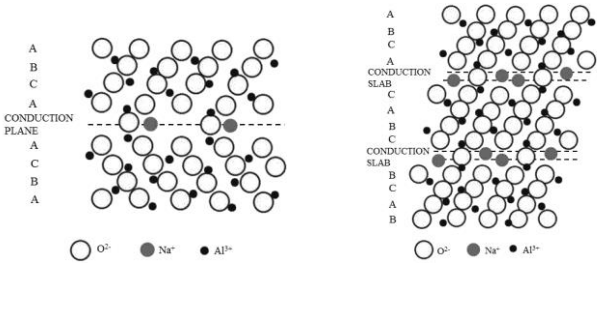

Fig. 2. Projection of a – β-Al_2O_3; b – β″-Al_2O_3 unit cells stacking sequence

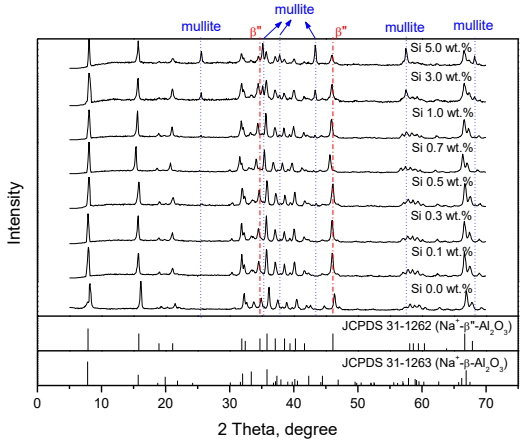

Fig. 3. XRD patterns of the synthesized SiO_2-doped Na^+-β/β″-Al_2O_3 powders, calcined at 1200 °C for 2 h

However, in the case of the 3 and 5 wt.% SiO_2-doped calcined powders, the mullite ($3Al_2O_3 \cdot 2SiO_2$) phase was detected. Fig. 4 shows the phase diagram for the binary Al_2O_3-SiO_2 system, produced by Aramaki and Roy [26], which demonstrates that the mullite phase appeared according to phase diagram for the binary Al_2O_3-SiO_2 system. The XRD patterns of the sintered specimens presented in Fig. 5 illustrate that after sintering, the Na^+-β/β″-Al_2O_3 phase was maintained, the mullite phase was not detected, and the $NaAlO_2$ and SiO_2 phases appeared in the 3 and 5 wt.% SiO_2-doped specimens. As a result of volatilization of Na_2O at high sintering temperature, the mullite reacted with Na_2O to generate the $NaAlO_2$ and SiO_2 phases.

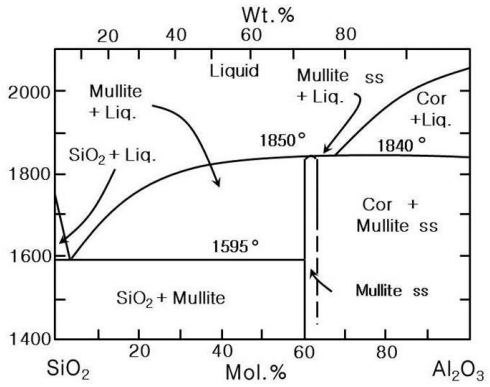

Fig. 4. Al_2O_3-SiO_2 binary phase diagram proposed by Aramaki and Roy [26]

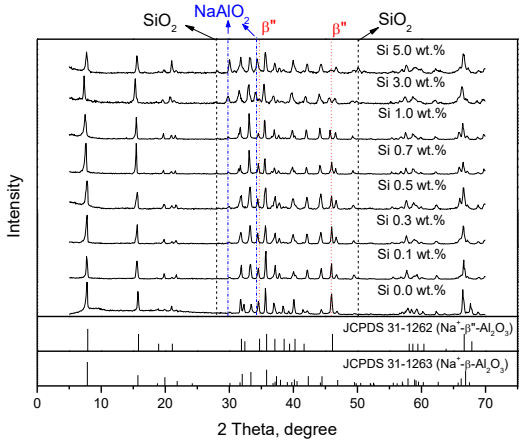

Fig. 5. XRD patterns of specimens sintered at 1600 °C for 30 min

Fig. 6 shows the phase fraction of the β″-Al_2O_3 analysis. Before sintering, the phase fraction of β″-Al_2O_3 was generally found to increase with increasing SiO_2 content. This trend is indicative of a tendency towards a rapid increase in the formation of the β″-Al_2O_3 phase in the 3 and 5 wt.% SiO_2-doped powders. As mentioned above, the theoretical formula of β-Al_2O_3 is $Na_2O \cdot 11Al_2O_3$, and the formula of β"-Al_2O_3 $Na_2O \cdot 5Al_2O_3$, therefore, in order to form the β"-Al_2O_3, it is necessary to more Na_2O than the case of forming the β-Al_2O_3. Due to the formation of the mullite ($3Al_2O_3 \cdot 2SiO_2$) phase, the molar ratio of Na_2O in the calcined powders increased, and this aided the formation of β″-Al_2O_3. In contrast, after sintering, the β″-Al_2O_3 fraction declined with increasing SiO_2 content, and the phase fraction of the β″-Al_2O_3 decreased significantly in the 3 and 5 wt.% SiO_2-doped specimens. Generally, the phase fraction of the β"-Al_2O_3 is decreased after sintering by a volatilization of Na_2O at high temperature. And Si in the Na^+-β/β″-Al_2O_3 led to an excess volatilization of the Na_2O to adjust the charge balance of the Na^+-β/β″-Al_2O_3. So, the phase fraction of β"-Al_2O_3 decline is attributed to transformation of β″-Al_2O_3 to β-Al_2O_3 via the volatilization of Na_2O, while the mullite phase reacted with Na_2O.

Fig. 7 shows the relative sintered density of the specimens sintered at 1650 °C for 30 min. The relative sintered density was improved by doping with small amounts of SiO_2. The relative sintered density of Na^+ β/β″-Al_2O_3 sintered specimen with 0.7 wt.% SiO_2 doping reached 99.2 % of the theoretical density. The increase in densification with SiO_2 content occurred partly by the effect of the liquid phase in allowing the rearrangement of the particles. A liquid phase creates an attractive force between the particles, putting the particle contacts in compression. This effect is so strong that complete densification is possible by rearrangement if enough volume fraction of liquid phase is present [27]. However, in the case of the 3 and 5 wt.% SiO_2-doped specimens, the relative sintered density declined. As the SiO_2 content increased, an excess of the liquid phase was formed relative to the liquid phase required for sintering, resulting in hindrance of the contact between the particles and the creation of pores due to the contraction of generated gas during cooling, thereby hampering the sintering process [28].

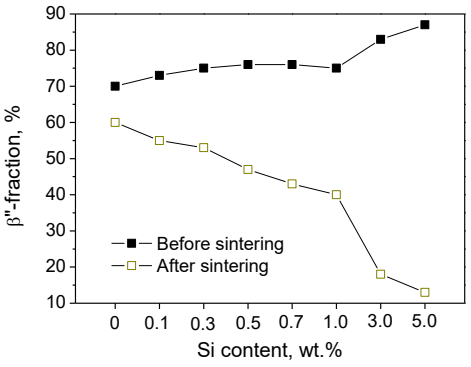

Fig. 6. β"-Al_2O_3 phase fraction of synthesized powder (before sintering) and sintered specimens (after sintering)

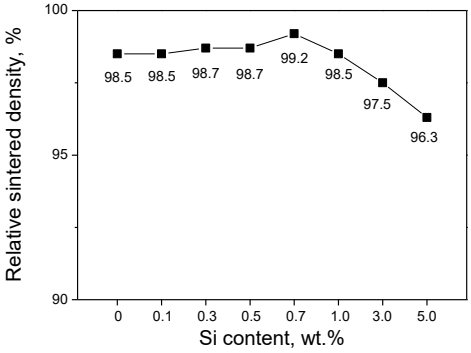

Fig. 7. Relative sintered density of specimens sintered at 1600 °C for 30 min as a function of SiO_2 content

Fig. 8 shows the Nyquist plot of the 0.7 SiO_2-doped sintered specimen at 225, 350 °C and 5.0 wt.% SiO_2-doped sintered specimen at 350 °C. Polycrystalline Na^+-β/β″-Al_2O_3 has grain bulk resistance (R_B) and grain boundary resistance (R_{GB}), so, it was possible to separate out the semi-circle part and the line part as shown in Fig. 8 a below 250 °C. But, the semi-circle part was substituted by some dots close to the Z' axis when the temperature was higher than 250 °C because the grain boundary or intergranular resistance became negligible at above 250 °C [29 – 31]. Na^+ ion in the Na^+-β/β″-Al_2O_3 conduct by jump mechanism between lattice sites of the conduction plane and slab, this jump mechanism is activated with rising temperature, so the grain boundary resistance contribution to the total electrolyte resistance becomes negligible above 250 °C [32, 33]. Thus, the Nyquist plot at 350 °C (Fig. 8 b, c) exists the grain bulk resistance, only.

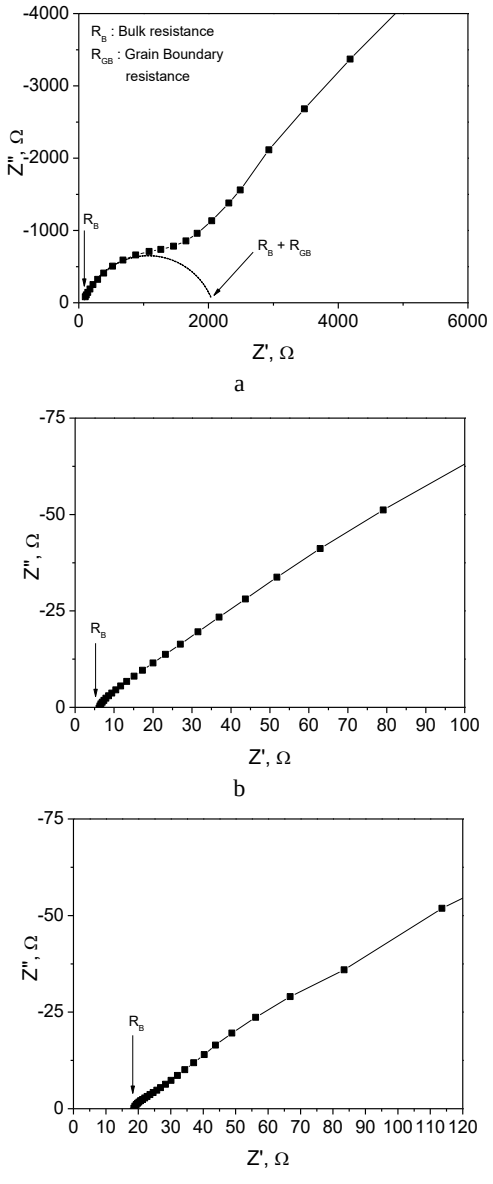

Fig. 8. Nyquist plot of the a – 0.7 wt.% SiO_2-doped sintered specimen at 225 °C; b – 0.7 wt.% SiO_2-doped sintered specimen at 350 °C; c – 5.0 wt.% SiO_2-doped sintered specimen at 350 °C

The measured bulk resistance at 350 °C of 5.0 wt.% SiO_2-doped sintered specimen was higher than the 0.7 wt.% SiO_2-doped sintered specimen.

The ionic conductivity of the specimens sintered at 1600 °C for 30 min is shown in Fig. 9. The relationship conformed to Arrhenius equation of $\sigma T = A\exp(-Ea/kT)$, where A is the pre-exponential and K is the gas constant and T is the absolute temperature. As shown, the activation energy (slope of graph) declines when the temperature is above 250 °C. It means that the resistance of Na^+ ion conductivity can be improved as the temperature increasing [34].

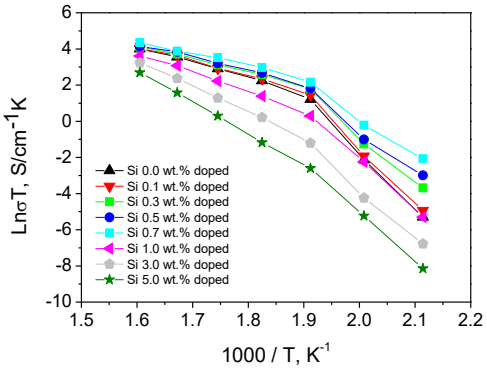

Fig. 9. Ionic conductivity of specimens sintered at 1600 °C for 30 min as a function of temperature in the range of 200 – 350 °C, with variation in the SiO_2 content

Although doping with a small amount of SiO_2 beneficially affects the ionic conductivity of the Na^+-β/β″-Al_2O_3 specimens, the addition of more than 1 wt.% SiO_2 leads to reduction in the ionic conductivity due to a decrease in the relative sintered density and formation of the $NaAlO_2$ and SiO_2 phases via transformation of β″-Al_2O_3 to β-Al_2O_3. The maximum ionic conductivity of 1.2×10^{-1} S/cm at 350 °C was achieved with the 0.7 wt.% SiO_2-doped specimen, and the minimum ionic conductivity was achieved with the 5.0 wt.% SiO_2-doped specimen with a value 2.4×10^{-2} S/cm at 350 °C. The ionic conductivities of Si-doped Na^+-β/β″-Al_2O_3 specimens at 350 °C are shown in Table 1.

Table 1. Ionic conductivities of Na^+-β/β″-Al_2O_3 specimens at 350 °C with various Si doping amounts

Dopant	Content, wt.%	Ionic Conductivity at 350 °C, S/cm
Si	0.0	8.8×10^{-2}
	0.1	8.8×10^{-2}
	0.3	9.8×10^{-2}
	0.5	1.0×10^{-1}
	0.7	1.2×10^{-1}
	1.0	6.0×10^{-2}
	3.0	4.1×10^{-2}
	5.0	2.4×10^{-2}

The phase fraction of β″-Al_2O_3 of 0.7 wt.% SiO_2-doped specimen was lower than the β″-fraction of specimen without doping, but the ionic conductivity of sintered specimens was enhanced with the inclusion of less than 0.7 wt.% SiO_2. So, it is supposed that the improved relative sintered density was the main cause for an increase in the ionic conductivity.

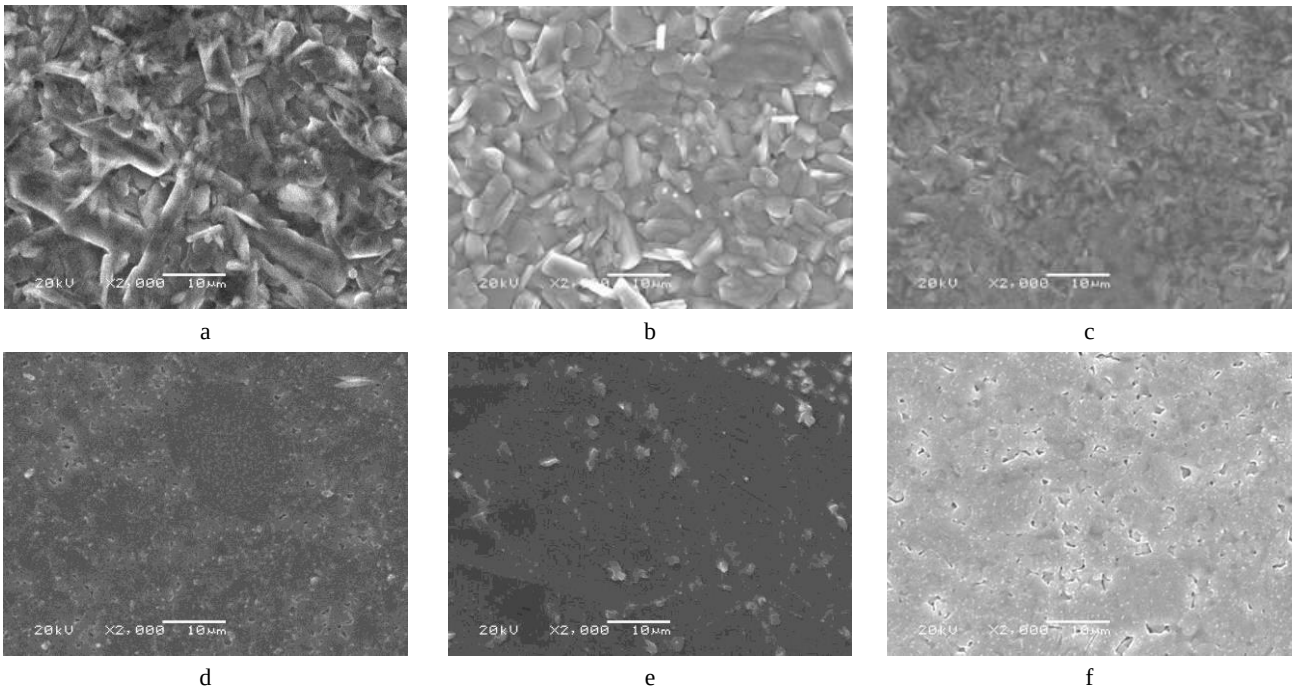

Fig. 10. SEM images of sintered specimens: a – SiO_2 0.1 wt.%-doped specimen (×2000); b – SiO_2 0.7 wt.%-doped specimen (×2000); c – SiO_2 5.0 wt.%-doped specimen (×2000); d – polished SiO_2 0.1 wt.%-doped specimen (×2000); e – polished SiO_2 0.7 wt.%-doped specimen (×2000); f – polished SiO_2 5.0 wt.%-doped specimen (×2000)

Na^+-β/β″-Al_2O_3 have interesting practical applicability because of their high ionic and low electronic conductivity. So, Na^+-β/β″-Al_2O_3 has been used as solid electrolyte in sodium/sulfur battery and this battery operate at 300 – 350 °C. Thus, the ionic conductivities data were focused at 350 °C, in this study [35, 36]. Table 2 lists ionic conductivity of various dopant doped Na^+-β/β″-Al_2O_3 investigated by other researchers for compared to the value obtained in this study [37 – 39].

Fig. 10 presents the SEM images of the specimens sintered at 1600 °C for 30 min. There is an apparent decrease in the grain size with increased SiO_2 doping.

Table 2. Ionic conductivities of various dopant doped Na^+-β/β″ Al_2O_3 specimens [37 – 39]

Dopant	Content	Ionic Conductivity, S/cm
Si (this study)	0.7 wt.%	1.2×10^{-1} (350 °C)
Ti	1.0 wt.%	2.1×10^{-1} (350 °C)
Zn	4.0 wt.%	8.0×10^{-2} (300 °C)
Co	4.0 wt.%	1.1×10^{-1} (300 °C)
Cu	4.0 wt.%	1.2×10^{-1} (300 °C)
Zr	15.0 vol.%	1.1×10^{-1} (300 °C)

This behavior may be attributed to a decline of the grain migration rate due to the formation of solid solutions at the grain boundaries [13]. Traces of liquid phase sintering with addition of excess SiO_2 in the entire region of the surface were confirmed from microstructural observation of the SiO_2 5.0 wt.%-doped specimen (Fig. 10 c), in contrast with the microstructure of the SiO_2 0.7 wt.%-doped specimen (Fig. 10 b). Fig. 10 f shows the microstructure of the polished SiO_2 5.0 wt.%-doped specimen. On the basis of the relative sintered density (96.3 %), this sample was somewhat porous compared to Fig. 10 d, e.

4. CONCLUSIONS

SiO_2-doped Na^+-β/β″-Al_2O_3 specimens were fabricated, and the changes in the properties of the Na^+-β/β″-Al_2O_3 solid electrolyte brought about by variation in the SiO_2 content of the doped samples were investigated. The mullite ($3Al_2O_3 \cdot 2SiO_2$) phase was observed in the case of the 3 and 5 wt.% SiO_2-doped Na^+-β/β″-Al_2O_3 powders. Volatilization of Na_2O at high sintering temperature and subsequent reaction with mullite generated the $NaAlO_2$ and SiO_2 phases in the 3 and 5 wt.% SiO_2-doped Na^+-β/β″-Al_2O_3 sintered specimens. In the sintered samples, the relative proportion of the β″-Al_2O_3 phase fraction declined with increasing addition of SiO_2; notably, the phase fraction of β″-Al_2O_3 declined severely in the 3 and 5 wt.% SiO_2-doped specimens. The relative sintered density was augmented by doping with small amounts of SiO_2, whereas, in the case of the 3 and 5 wt.% SiO_2-doped specimens, the relative sintered density decreased. It is deduced that increasing the SiO_2 content lead to excessive liquid phase formation during sintering, and this excessive liquid phase hindered inter-particle contact with consequent formation of pores. The ionic conductivity was enhanced by doping with a small amount of SiO_2, whereas the addition of more than 1 wt.% SiO_2 leads to a decrease in the ionic conductivity due to the phase relationship and reduction in the relative sintered density. In conclusion, the properties of Na^+-β/β″-Al_2O_3 were improved by inclusion of less than 0.7 wt.% SiO_2.

Acknowledgments

This paper was supported by Konkuk University in 2017.

REFERENCES

1. **Kummer, J. T.** β-alumina Electrolytes *Progress in Solid State Chemistry* 7 1972: pp. 141 – 175. https://doi.org/10.1016/0079-6786(72)90007-6
2. **Battles, J. E.** Materials for Advanced High Temperature Secondary Batteries *International Materials Reviews* 34 1989: pp. 1 – 18. https://doi.org/10.1179/imr.1989.34.1.1
3. **Johnson, Jr,D.W., Granstaff, S.M., Rhodes, W.W.** Preparation of β″-Al_2O_3 Pressing Powders by Spray Drying *Ceramic Bulletin* 58 (8) 1979: pp. 849 – 852.
4. **Hodge, J.D.** Powder Processing and Crystallization of β and β″ Aluminas *American Ceramic Society Bulletin* 62 1983: pp. 244 – 248.
5. **Choy, J.H., Yoo, J.S., Han, Y.S., Kim, Y.H.** Citrate Sol-Gel Method for The Preparation of β/β″-Alumina *Materials Letters* 16 1993: pp. 226 – 230. https://doi.org/10.1016/0167-577X(93)90169-X
6. **Youngblood, G., Vircar, A.V., Cannon, W.R., Gordon, R.S.** Sintering Process and Heat Treatment Schedules for Conductive, Lithia-Stabilized Beta Double Prime-Al_2O_3 *American Ceramic Society Bulletin* 56 1977: pp. 206 – 210.
7. **Miller, M.L., Mcentire, B.J., Miller, G.R., Godon, R.S.** A Prepilot Process for the Fabrication of Polycrystalline β″-Alumina Electrolyte Tubing *American Ceramic Society Bulletin* 58 1979: pp. 522 – 524.
8. **Rivier, M., Pelton, A.D.** A New Slip Casting Technique for The Laboratory Fabrication of β-Al_2O_3 and Other Ceramics *American Ceramic Society Bulletin* 56 1978: pp. 183 – 185.
9. **Powers, R.W.** Ceramic Aspects of Forming Beta Alumina by Electrophoretic Deposition *American Ceramic Society bulletin* 65 1986: pp. 1270 – 1277.
10. **Koyama, T., Nishiyama, A., Niihara, K.** Effect of a Small Amount of Liquid-Forming Additives on the Microstructure of Al_2O_3 Ceramics *Journal of Materials Science* 28 1993: pp. 5953 – 5956. https://doi.org/10.1007/BF00365207
11. **Kaysser, W.A., Sprissler, M., Handwerker, C.A., Blendell, J.E.** Effect of a Liquid Phase on the Morphology of Grain Growth in Alumina *Journal of the American Ceramic Society* 70 (5) 1987: pp. 339 – 343. https://doi.org/10.1007/BF00365207
12. **Erkalfa, H., Nisirli, Z., Baykara, T.** The Effect of TiO_2 and MnO_2 on Densification and Microstructural Development of Alumina *Ceramics International* 24 1998: pp. 81 – 90. https://doi.org/10.1016/S0272-8842(97)00082-5
13. **Louet, N., Fantozzi, G., Reveron, H.** Sintering Behaviour and Microstructural Evolution of Ultrapure A-Alumina Containing Low Amounts of SiO_2 *Journal of the European Ceramic Society* 28 2008: pp. 205 – 215. https://doi.org/10.1016/j.jeurceramsoc.2007.04.015
14. **Svancarek, P., Lendvayova, S., Galusek, D., Hnatko, M., Vavra, I., Wang, X.** Abrasive Wear Resistance of SiO_2-Doped Polycrystalling Alumina *Wear* 271 2011: pp. 760 – 769. https://doi.org/10.1016/j.wear.2011.03.016
15. **Kwon, O.S., Hong, S.H., Lee, J.H., Chung, U.J., Kim, D.Y., Hwang, N.M.** Microstructural Evolution During Sintering of TiO_2/SiO_2-doped Alumina: Mechanism of Anisotropic Abnormal Grain Growth *Acta Materialia* 50 (19) 2002: pp. 4865 – 4872. https://doi.org/10.1016/S1359-6454(02)00355-5
16. **Moshe, R., Berner, A., Kaplan, W.D.** The Solubility Limit of SiO_2 in α-alumina at 1600 ℃ *Scripta Materialia* 86 2014: pp. 40 – 43. https://doi.org/10.1016/j.scriptamat.2014.05.005
17. **Louet, N., Gonon, M., Fantozzi, G.** Influence of the Amount of Na_2O and SiO_2 on the Sintering Behaviour and on the Microstructural Evolution of a Bayer Alumina Powder *Ceramics International* 31 (7) 2005: pp. 981 – 987. https://doi.org/10.1016/j.ceramint.2004.10.013
18. **Woo, K.D., Huo, H.W.** Effect of High Energy Ball Milling on Displacement Reactin and Sintering of Al-Mg/SiO_2 **C**omposite Powders *Metals and Materials International* 12 2006: pp. 45 – 50. https://doi.org/10.1007/BF03027522
19. **Schmid, C.** X-ray Characterization of β- and β″-alumina *Journal of Materials Science Letters* 5 (3) 1986: pp. 263 – 266. https://doi.org/10.1007/BF01748072
20. **Lee, S.T., Kim, S.G., Jang, M.H., Hwang, S.H., Haw, J.R., Lim, S.K.** Analysis of the Phase Formation of Na- β/β″-Aluminas using MgO and Li_2O as Phase Stabilizers *Journal of Ceramic Processing Research* 12 2011: pp. 38 – 45.
21. **Yamaguchi, G., Suzuki, K.** On the Structures of Alkali Polyaluminates *Bulletin of the Chemical Society of Japan* 41 1968: pp. 93 – 99. https://doi.org/10.1246/bcsj.41.93
22. **De Kroon, A.P., Schafer, G.W., Aldinger, F.** Direct Synthesis of Binary K-β-and K-β″-alumina. 1. Phase Relations and Influence of Precursor Chemistry *Chemistry of Materials* 7 1995: pp. 878 – 887. https://doi.org/10.1021/cm00053a011
23. **Yao, Y.Y., Kummer, J.T.** Ion Exchange Properties of and Rates of Ionic Diffusion in Beta-alumina *Journal of Inorganic and Nuclear Chemistry* 29 (9) 1967: pp. 2453 – 2475. https://doi.org/10.1016/0022-1902(67)80301-4
24. **Certo, J., Furtado, C.S., Ferreira, A.J., Perdigao, J.M.** Na- β Alumina Powder Processing by a Na_2CO_3 Precipitation Method *Ionics* 4 (1) 1998: pp. 124 – 128. https://doi.org/10.1007/BF02375790
25. **Fally, J., Lasne, C., Lazennec, Y., Le Cars, Y., Margotin, P.** Study of a Beta-alumina Electrolyte for Sodium-sulfur Battery *Journal of the Electrochemical Society* 120 (10) 1973: pp. 1296 – 1298.
26. **Aramaki, S., Roy, R.** The Mullite-Corundum Boundary in The Systems MgO-Al_2O_3-SiO_2 and CaO-Al_2O_3-SiO_2 *Journal of the American Ceramic Society* 42 (12) 1959: pp. 644 – 645. https://doi.org/10.1111/j.1151-2916.1959.tb13589.x
27. **Borsa, C.E., Ferreira, H.S., Kiminami, R.H.G.A.** Liquid Phase Sintering of Al_2O_3/SiC Nanocomposites *Journal of the European Ceramic Society* 19 (5) 1999: pp. 615 – 621. https://doi.org/10.1016/S0955-2219(98)00252-0
28. **Park, S.H., Park, W.J., Yoon, H.K.** Wear Characteristics of Sic by Sintered Temperature and SiO_2 Contents *Transactions of the Korean Society of Mechanical Engineers A* 32 2008: pp. 1003 – 1009.

29. **Sudwotrh, J.L., Tilley, A.R.** The Sodium Sulfur Battery *Champman and Hall Ltd. London* 1985: pp. 21 – 47.
30. **Lin, J., Wen, Z., Wang, X., Song, S., Liu, Y.** Mechanochemical Synthesis of Na^+-β/β″-Al_2O_3 *Journal of Solid State Electrochemistry* 14 2010: pp. 1821 – 1827. https://doi.org/10.1007/s10008-010-1053-5
31. **Hooper, A.** A Study of the Electrical Properties of Single-Crystal and Polycrystalline β-alumina Using Complex Plane Analysis *Journal of Physics D: Applied Physics* 10 1977: pp. 1487 – 1497.
32. **De Jonghe, L.C.** Grain Boundaries and Ionic Conduction in Sodium Beta Alumina *Journal of Materials Science* 14 1979: pp. 34 – 48. https://doi.org/10.1007/BF01028326
33. **Rohrer, C.L., Farrington, G.C.** Molecular Dynamics Simulation of the Temperature-Dependent Ionic Conductivity in Sodium(I)-β″-alumina *Chemistry of Materials* 4 1992: pp. 55 – 62. https://doi.org/10.1021/cm00019a014
34. **Xu, D., Jiang, H., Li, M., Hai, O., Zhang, Y.** Synthesis and Characterization of Y_2O_3 Doped Na^+-β″-Al_2O_3 Solid Electrolyte by Double Zeta Process *Ceramics International* 41 2015: pp. 5355 – 5361. https://doi.org/10.1016/j.ceramint.2014.12.094
35. **Lu, X., Xia, G., Lemmon, J. P., Yang, Z.** Advanced Materials for Sodium-Beta Alumina Batteries: Status, Challenges and Perspectives *Journal of Power Sources* 195 2010: pp. 2431 – 2442. https://doi.org/10.1016/j.jpowsour.2009.11.120
36. **Lee, D.H., Lee, S.T., Lee, K.M., Lim, S.K.** Analysis of the Crystal Phases of Na^+-beta-aluminas Synthesized by Infiltration of Alkali Molten Salts *Journal of Industrial and Engineering Chemistry* 18 2012: pp. 1801 – 1806. https://doi.org/10.1016/j.jiec.2012.04.006
37. **Yang, L.P., Shan, S.J., Wei, X.L., Liu, X.M., Yang, H., Shen, X.D.** The Mechanical and Electrical Properties of ZrO_2-TiO_2-Na^+-β/β″-alumina Composite Electrolyte Synthesized Via a Citrate Sol-Gel Method *Ceramics International* 40 2014: pp. 9055 – 9060. https://doi.org/10.1016/j.ceramint.2014.01.118
38. **Sheng, Y., Sarkar, P., Nicholson, P.S.** The Mechanical and Electrical Properties of ZrO2- Na^+-β″-Al_2O_3 Composites *Journal of Materials Science* 23 1988: pp. 958 – 967. https://doi.org/10.1007/BF01153995
39. **Wasiucionek, M., Garbarczyk, J., Jakubowski, W.** Electrical properties of CoO, NiO, CuO and ZnO Doped Beta″-alumina *Solid State Ionics* 7 1982: pp. 283 – 286. https://doi.org/10.1016/0167-2738(82)90024-8